Signals In Temperature Extremes Emerge in China During The Last Millennium Based On CMIP5 and CMIP6 Simulations

Yue Sui (suiyue@cug.edu.cn)
China University of Geosciences https://orcid.org/0000-0002-5464-6486
Yuting Chen
China University of Geosciences

Research Article

Keywords: signal-to-noise ratio, temperature extremes, simulation, China

Posted Date: December 1st, 2021

DOI: https://doi.org/10.21203/rs.3.rs-1085891/v1

Abstract

Though the magnitude of any change is important, regions which have a larger signal of change relative to the background variations will potentially face greater risks than other regions, as they will see unusual or novel climate conditions more quickly (Frame et al. 2017). Providing more information about signal and noise on regional scales, and the associated attribution to particular causes, is therefore important for adaptation planning (Chen et al. 2021). However, whether a detectable signal in temperature extremes emerges in China at the local or regional level during 850–2005 has not been discussed. Based on six selected and bias-corrected global models under the Coupled Model Intercomparison Project phase 5, relative to pre-industrial levels (ca 1850), we show that the temporal information of signal-to-noise ratio (S/N) in annual temperature extremes are consistent with annual mean temperature variations in China during 850–2005. Before 1850, absolute values of regional mean S/N in temperature extremes under cold climatic conditions are generally larger than that under warm climatic conditions. At the level of S/N > 1, local increasing signals of cold extremes emerge in the second half of 13th century and in the early 19th century after intensively volcanic eruptions in 1257 and 1815 in most part of China, especially in southern China and Tibet Plateau. Over the past 150 years under global warming, absolute values of regional mean S/N in temperature extremes have increasing trends. The regional mean increasing signals of warm extremes over China begin to exceed natural variability in 1969 at the level of S/N > 1, and local warm signals first occur in 1929 in Tibet Plateau. These warming signals are related to greenhouse gas forcing.

Introduction

Knowledge of the temperature variability during the last one to two millennia provides a context for future climate change and is important for determining climate sensitivity and the processes that control warming. Since systematic instrumental temperature records only extend back to the 19th century, such knowledge mainly relies on proxy data and model simulations.

Over the past two decades, many proxy-based temperature reconstructions in East Asia or China covering the past one to two millennia have been published (Yang et al. 2002; Wang et al. 2007; Cook et al. 2013; Ge et al. 2013; Shi et al. 2015; Zhang et al. 2018). The temperature reconstructions generally show a warm period during the first two centuries AD, followed by a multi-century long cooling period, again a warm condition from ca 900 to 1200 AD (Medieval Climate Anomaly), and a cooler climate from about 1450 to 1850 AD (Little Ice Age). The last 150 years are characterized by a continuous warming until recent time. This shows a similar behavior to that of the northern hemisphere (Christiansen and Ljungqvist 2017). Moreover, three field temperature reconstructions over East Asia have recently been published, which can offer temporal and spatially resolved information over past temperature variability (Cook et al. 2013; Shi et al. 2015; Zhang et al. 2018). The field temperature reconstructions generally compare well with the ensemble model simulation of the Coupled Model Intercomparison Project Phase 5 (CMIP5) during 850–2005 (Masson-Delmotte et al. 2013; Zhang et al. 2018).

Meanwhile, some extreme climate events reconstructions in China have been made. For example, Zhang and Gaston (2004) reports 19 extreme burning hot summers in the last 1000 years by surveying weather and related impact records from “A Compendium of Chinese Meteorological Records of the Last 3000 years” (Zhang 2004). For example, the northern China heat wave in summer 1743 is the greatest in intensity, injuries, area of coverage and duration, and another one extreme burning hot summer is in 1215. Hao et al. (2011) identifies historical analogues of the central and southern Chinese 2008 extreme snow event from the chronology of extremely cold winters reconstructed over the last 500 years. Zheng et al. (2012) identifies 50 extreme cold winters for the period 1650–1949 based on 4000 pieces of comparable information extracted from local gazettes in southern China. Lyu et al. (2016) reconstructs April–July minimum temperature on Laobai Mountain during the past 414 years.

The early onset of sustained, significant warming in paleoclimate records and model simulations suggests that greenhouse gas forcing of industrial-era warming commenced as early as the mid-19th century (Abram et al. 2016). Since the Intergovernmental Panel on Climate Change Third’s Assessment report in 2001, the observed signal of climate change has been unequivocally detected at the global scale, and this signal is increasingly emerging from the noise of natural variability on smaller spatial scales and in a range of climate variables (Chen et al. 2021). Nevertheless, most researches about time of emergence in mean and extreme climate are focused on the period of the last 150 years and the future, based on instrumental records and model simulations (Giorgi and Bi 2009; Mahlstein et al. 2011; Hawkins and Sutton 2012; Mora et al. 2013; Sui et al. 2014; King et al. 2015; Lopez et al. 2018; Nguyen et al. 2018). However, to the best of our knowledge, whether a detectable signal in temperature extremes emerges at the local or regional level during the last millennium has not been discussed.

One approach to doing this utilizes the signal-to-noise ratio (S/N) which is the ratio of signal in temperature extremes to its natural variability (Hawkins and Sutton 2012). The S/N describes the magnitude of the climate change signal relative to its natural variability and may be useful for climate impact assessments. Though the magnitude of any change is important, regions which have a larger signal of change relative to the background variations will potentially face greater risks than other regions, as they will see unusual or novel climate conditions more quickly (Frame et al. 2017). The S/N is also important for many hazards (Loarie et al. 2009). Providing more information about signal and noise on regional scales, and the associated attribution to particular causes, is therefore important for adaptation planning (Chen et al. 2021).

Therefore, the purpose of this study is to address whether signals in temperature extremes over China exceed its natural variability during the last millennium and if yes where and when the signals will occur first.

Data And Methods

2.1 Data

Daily minimum and maximum near-surface air temperatures of seven global climate models from the CMIP5 of the World Climate Research Programme and two CMIP6 models are available at this stage. All seven models from CMIP5 have performed the pre-industrial control run, the 20th century experiment with all forcing (or historical run) and the last millennium experiment (or past1000 run) described by Taylor et al. (2012), and similar information of two CMIP6 models is described by Eyring et al. (2016). These climate model data are freely accessible at the website https://esgf-node.llnl.gov/search/. We use only the first run for each model to treat all of the models equally. Basic information on the nine models and their experiments is presented in Table 1.

To bias correct the performance of models in simulating climate extremes over China, we used observation data for daily minimum and maximum temperatures at the 0.25° × 0.25° horizontal resolution during the period 1961–2005. It is constructed from 2416 observation stations over China by the National Climate Center of the China Meteorological Administration (Wu and Gao 2013, hereafter referred to as CN05.1).

To compare paleoclimate data with model simulations, surface air temperatures at the 2° × 2° horizontal resolution from 20 ensemble-mean values for each Monte-Carlo reconstruction of Last Millennium Reanalysis (LMR) version 2 are used in our work. The LMR version 2 utilizes an ensemble methodology to assimilate paleoclimate data for the production of annually resolved climate field reconstructions of the Common Era, which is based on an updated proxy database and seasonal regression-based forward models (Tardif et al. 2019).

Given the range of horizontal resolutions of the nine models and observation data, all of simulations and observation data are regridded to a relatively mid-range horizontal grid resolution of 2° × 2°. Seasonal analyses were performed according to standard procedures for winter (December–January–February, DJF) and summer (June–July–August, JJA).

2.2 Climate extreme indices

We considered 12 indices of temperature extremes in this work (Table 2). They are the coldest night (TNn), the warmest night (TNx), tropical nights (TR), frost days (FD), warm nights (TN90p), and cold nights (TN10p), which are based on daily minimum temperature, and the coldest day (TXn), the hottest day (TXx), summer days (SU), icing days (ID), warm days (TX90p), and cold days (TX10p), which are based on daily maximum temperature. The indices are generally divided into absolute indices (TNn, TNx, TXn, and TXx), absolute threshold indices (TR, FD, SU, and ID), and percentile-based threshold indices (TN90p, TN10p, TX90p, and TX10p). The percentile-based threshold indices are based on percentiles calculated from 5-day windows centred on each calendar day in the reference period. TN10p and TX10p (TN90p and TX90p) are based on the 10th (90th) percentile during the baseline period 1961–1990 in this work. To avoid possible inhomogeneity across the in-base and out-base periods, a bootstrap procedure recommended by Zhang et al. (2005) is taken for the baseline period 1961–1990. Detailed information on the indices can be found in Sillmann et al. (2013), or on the ETCCDI website http://etccdi.pacifcclimate.org/list_27_indices.shtml.

2.3 Bias-correcting daily minimum and maximum temperatures of models

First, we assess whether these models could satisfactorily reproduce the trend in regional mean temperature over China during 850–2005. One CMIP5 model (MIROC-ESM) presents an increasing trend during 850–1850, since it shows a problematic long-term drift (Fig. S1, Bothe et al. 2013; Sueyoshi et al. 2013). This is opposite to proxy-based temperature reconstructions (Yang et al. 2002; Wang et al. 2007; Cook et al. 2013; Ge et al. 2013; Shi et al. 2015; Zhang et al. 2018). In addition, this CMIP5 model and two CMIP6 models (MRI-ESM2-0 and EC-Earth3-Veg-LR) cannot capture the warm period during the 20th century (Fig. S1). To be specific, the simulated temperature during 1850–2005 is lower than that during 850–1849 for these three models (Fig. S1). Thus, the outputs of MIROC-ESM and two CMIP6 models are not used and only six models of CMIP5 are selected in next analysis.

Second, the level of confidence in past and future climate based on a climate model depends in part on the skill of the model in reproducing the current observed climate. According to Li et al. (2020), we use a simple ‘Δ-method’ to reduce the bias of model-derived daily minimum or maximum temperature relative to observation from CN05.1. To estimate the bias, the seasonal cycle of daily minimum or maximum temperature obtained from 45-year CN05.1 dataset (1961–2005) is subtracted from the seasonal cycle calculated with model historical (1961–2005) simulations. The resulting bias in the seasonal cycle is then removed from daily minimum or maximum temperature calculated from the output of model simulations. Then, all of indices of climate extremes are calculated based on the bias-corrected daily minimum and maximum temperatures. Although only the seasonal cycles of daily minimum and maximum temperatures are bias-corrected, most of climate extremes from bias-corrected model simulations show an overall close resemblance with those from CN05.1 (Fig. S2–S3).

2.4 Signal-to-noise ratio

The S/N is an important metric for comparing local signals with natural variability (Hawkins and Sutton 2012). First, the modeling periods of pre-industrial control run shown in Table 1, in which external forcings are fixed at non-evolving pre-industrial conditions (Taylor et al. 2012), are considered as the reference period. Relative to the pre-industrial level, the time series of the signal of each model from 850–2005 is indicated by a change in 31-year running average, a time period that is sufficient to filter out inter-annual variability (Sui et al. 2018). For example, the signal at year 865 is the difference between the mean of the period 850–880 and mean of the reference period.

Second, consistent with the definition from Hawkins and Sutton (2012), the internal variability of a climate system is considered “climate noise”. The natural variability of the climate system occurs in the absence of external forcing and includes processes intrinsic to the atmosphere, the ocean and the coupled ocean–atmosphere system, such as El Niño-Southern Oscillation, Atlantic Multidecadal Oscillation, and Pacific Decadal Oscillation (Deser et al. 2012). The pre-industrial control simulation from each model is used to estimate the noise, which is defined as the inter-annual standard deviation of the annual or seasonal means (Sui et al. 2018).

Then, the signal and the noise of temperature extremes are calculated separately for each model at each grid cell. Thus, the S/N of each temperature extreme is obtained from the ratio of signal to noise in each temperature extreme for each model or CMIP5 multi-model median in each grid cell. In our work, we consider that signals emerge from natural variability or it is outside natural variability, when its absolute value of S/N is larger than 1.

Lacking of pre-industrial control run for LMR, the pre-industrial period 1651–1850 is considered as the reference period. Then, relative to the period 1651–1850, the time series of the signal of each ensemble-mean values for each Monte-Carlo reconstruction from 850–2000 is indicated by a change in 31-year running average. Third, the noise in annual mean temperature for LMR is the standard deviation of annual mean temperature during the period 1651–1850. Finally, the time series of S/N in annual mean temperature for each ensemble-mean values for each Monte-Carlo reconstruction from 850–2000 and their median are calculated based on the signal and noise.

Results

3.1 The S/N in annual temperature extremes during 850–2005 in China relative to the pre-industrial level

3.1.1 Mean temperature

First, time series of area-weighted regional mean S/N in annual mean temperature during 850–2005 over the land grid point of China for bias-corrected six CMIP5 models and their multi-model median relative to the pre-industrial level are shown in Fig. 1a. The S/N in annual minimum and maximum temperatures have similar features to annual mean temperature during 850–1850 (Fig. S4a). Before 1850, regional mean multi-model median S/N in annual mean temperature over the whole China are from –0.8 to 0.1. In other words, regional mean changes in annual mean temperature over China do not exceed natural variability during 850–1850 at the level of S/N > 1, based on the multi-model median S/N.

Nevertheless, annual cold signals in periods 1245–1303, 1446–1461, 1597–1614, 1647–1650, 1684–1727, and 1801–1829 emerge from natural variability at the level of S/N > 1 at local scale (Fig. 2a). For example, during 1245–1303, 1684–1727, and 1801–1829, the proportions of the areas where the multi-model median S/N in annual mean temperature are smaller than –1 to the whole country are from 0.4% to 25.1%, from 0.4% to 11.0% and from 0.5% to 4.9%, respectively. These large S/N may be driven by volcanic events (Fig. 1d), particularly after the large eruptions in 1257, 1452, 1600, and 1815 (Hartl-Meier et al. 2017). The results from six individual models are similar to the multi-model median except CSIRO-Mk3L-1-2, which has some warm signals in annual mean temperature during 850–1850. In addition, CCSM4, IPSL-CM5A-LR, and MPI-ESM-P have stronger signals than multi-model median and the other three models with respect to volcanic forcing during 850–1850 (Fig. 1a and Fig. 2a).

During the period 1851–2005, regional mean signal in annual minimum, mean, and maximum temperature begins to be larger than natural variability in 1971, 1972, and 1980 at the level of S/N > 1, respectively (Fig. 1a and Fig. S4a). At local scale, the warm signals in annual mean, minimum and

maximum temperatures begin to emerge in 1929, 1933, and 1944 at the level of S/N > 1, respectively, and occur in most of China until 2005 (Fig. 2a and Fig. S4a). These warm signals are mainly caused by greenhouse gas forcing (Fig. 1a and Fig. 1d, Schmidt et al. 2011). All six individual models have warm signals in the 20th century, and the time of emergence in signals in annual temperature for IPSL-CM5A-LR is earlier than that for other five models at the level of S/N > 1 (Fig. 1a).

Next, S/N in annual mean temperature from CMIP5 models are compared with that from LMR. On one hand, median signals in annual mean temperature of LMR over China do not emerge from natural variability at the level of S/N > 1, either (Fig. 1a). Specifically, median regional mean S/N in annual mean temperature from LMR over China during 850–1850 are in the range of –0.7 to 0.6. Moreover, the correlation coefficient between median S/N in annual mean temperature from CMIP5 models and that from LMR during 1400–1850 (0.25) is higher than that during 850–1399 (–0.30). In addition, both of them show that the early 19th century is a cold period. However, local signals from the median runs of LMR do not emerge from natural variability during 850–1850 after the volcanic forcing in the CMIP5. On the other hand, during period 1851–2005, both CMIP5 simulations and LMR have the increasing trend for S/N in annual mean temperature, and their correlation coefficient is 0.87 (Fig. 1a). Nevertheless, the time of emergence in median regional mean signals of annual mean temperature over China for LMR is 10 years later than that for CMIP5 models at the level of S/N > 1.

3.1.2 Cold extremes

The temporal information of annual cold nights (TN10p) is consistent with annual mean temperature variations in China, with larger (smaller) S/N in cold (warm) climatic conditions before 1850 (Fig. 1a and Fig. 1b). The regional mean S/N in annual cold nights range from 0.1 to 1.5 before 1850. Specially, during both 1247–1276 and 1810–1828, regional mean S/N in annual cold nights in China are larger than 1. At local scale, the increasing signals in annual cold nights emerge from natural variability in the 13th century and from the end of 16th century to the first half of 19th century at the level of S/N > 1. It is worth mentioning that during 1261–1276 and 1817–1827 the increasing signals in annual cold nights emerge from natural variability in more than half of China at the level of S/N > 1. The correlation coefficient between S/N of cold nights and radiative forcing from volcanic aerosols is –0.50, –0.95, and –0.54 during the period 900–1200, 1201–1449, and 1450–1850, respectively, and the correlation coefficients between multi-model median S/N of cold nights and other radiative forcings are low (Table 3). The results from six individual models are also similar to the multi-model median during 850–1850 except that CSIRO-Mk3L-1-2 has some warm signals in annual cold nights, and that CCSM4, IPSL-CM5A-LR, and MPI-ESM-P have stronger signals than multi-model median and the other three models with respect to volcanic forcing at the level of S/N > 1 (Fig. 1b and Fig. 2b).

During 1851–2005, regional mean median S/N in annual cold nights in China are from –1.2 to 0.4, with decreasing signals exceeding natural variability from 1984 (Fig. 1b). All six individual models also have decreasing signals in annual cold nights, and the time of emergence in signals of annual cold nights for

IPSL-CM5A-LR is earlier than that for other five models (Fig. 1b). Local decreasing signals in annual cold nights emerge from noise in 1970s for multi-model median (Fig. 2b).

The other cold extreme indices, such as cold days (TX10p), frost days (FD), and icing days (ID) have similar features to cold nights (TN10p), but their absolute values of S/N are generally smaller than that of cold nights (Fig. S4c–S4d). To be specific, regional mean increasing signals in annual cold nights and cold days over China emerge from natural variability during 1247–1276 and 1810–1828, and there are no regional mean signals in other temperature extremes for the whole country before 1850. At local scale, the increasing signals in annual cold nights, cold days, frost days, and icing days exceed natural variability in the second half of the 13th century and in the early 19th century. The local increasing signals in annual cold nights and cold days are outside natural variability from the end of the 16th century to the end of the 18th century.

Compared to the identification about the extreme cold winter events in southern China during 1650–2000 from Zheng et al. (2012), it is consistent that low frequency cold nights (TN10p) in winter in southern China occurs in 1730–1800 and in the second half of the 20th century (Fig. S5a). Both of them show that high frequency cold nights in winter in southern China occurs in 1800–1850 (Fig. S5a), but simulation presents that the first half of this period has more cold nights than the second part has, and that is opposite to Zheng et al. (2012). In addition, they find the intensities of some cold events in southern China are strong, such as those during 1653–1654, 1670, 1690, 1861, 1892 and 1929. The simulation can reproduce that both in 1690 and in 1892, with a weak magnitude (Fig. S5b–S5c).

3.1.3 Warm extremes

The warm extreme indices, such as warm days (TX90p), summer days (SU), tropical nights (TR), hottest day (TXx), and warmest night (TNx) have similar features to warm nights (TN90p), but their absolute values of multi-model median S/N are generally smaller than that of warm nights (Fig. S4b–S4d). Consistent with annual mean temperature changes, larger (smaller) absolute values of multi-model median S/N in warm nights occur in cold (warm) climatic conditions during 850–1850 (Fig. 1a and Fig. 1c). However, there are no regional mean multi-model median signals in these warm extremes for the whole country before 1850, with regional mean multi-model median S/N in annual warm extremes being from −0.6 to 0.03. At local scale, the decreasing signals in annual TNx and TR exceed natural variability in the second half of the 13th century and in the early 19th century. The local decreasing signals in annual TNx are also larger than natural variability in the middle of the 15th century. For individual models, CCSM4, IPSL-CM5A-LR, and MPI-ESM-P have decreasing signals in warm nights with respect to volcanic forcing during 850–1850 (Fig. 1c and Fig. 2c).

As for multi-model median results, regional mean increasing signals in annual warm nights, warm days, and tropical nights for the whole country emerge from natural variability during 1851–2005, with the regional mean signals first occurring in 1969 for annual warm nights (Fig. 1c, and Fig. S4c–S4d). There are some local signals in almost all annual warm extremes during 1851–2005, with local signals first occurring in 1929 for annual warm nights (Fig. 2c, and Fig. S4b–S4d). The local increasing signals in

annual warm nights emerge from natural variability until 1989 for all grid points of the whole country (Fig. 2c). All six individual models also have increasing signals in annual warm nights, and the time of emergence in signals of annual warm nights for IPSL-CM5A-LR is earlier than that for other five models (Fig. 1c, and Fig. 2c).

According to the research of Zhang and Gaston (2004), the northern China heat wave in summer 1743 is severe, and another strong case is in 1215. From the view of S/N, the signals of summer maximum temperatures in 1215 and 1743 do not exceed natural variability over China based on simulation (Fig. S6). Moreover, models cannot capture the features of hot events in 1215, but represent a weakly warmer summer in northern China in 1743 (Fig. S6b–S6c). The other warm extreme indices have similar results with summer maximum temperature (Fig. S6d–S6e).

3.2 The S/N in annual temperature extremes in subregion of China relative to the pre-industrial level

We examine the spatial patterns of S/N in temperature extremes by dividing China into four roughly equal area land regions, including northwestern China (NWC), northeastern China (NEC), Tibet Plateau (TP), and southern China (SC) (Fig. 3). On one hand, the noise variance decreases with averaging (Hawkins and Sutton 2012). On another hand, these regions were determined by annual mean temperature (Fig. 3a), noise of temperature extremes (Fig. 3b–3c), administrative boundaries and societal and geographical conditions.

Time series of area-weighted regional mean S/N in annual mean temperature, cold nights, and warm nights during 850–2005 over the land grid point of four regions in China for multi-model median relative to the pre-industrial level are shown in Fig. 4. The multi-model median S/N in annual mean and extreme temperatures in subregions of China during 850–1850 have similar features to that in China (Fig. 4–5). The annual mean and extreme temperatures have some differences among four regions with respect to volcanic forcing during 850–1850 (Fig. 4–5). For example, northeastern China has local signals in annual cold nights with respect to strong volcanic forcing, such as after the large eruptions in 1257 and 1815; northwestern China, Tibet Plateau, and southern China have local signals in annual cold nights with respect to both weak and strong volcanic forcing (Fig. 1d and Fig. 5b). The other cold extremes, such as cold days, frost days, and icing days, have similar regional features during 850–1850, but their areas where signals emerge from natural variability are smaller than that for cold nights (Fig. S7). Compared our results with the reconstruction by Li et al. (2021), both of them show that the early 19th century is a cold period in Tibet.

As for warm signals during the 20th century, the time of emergence in signals of annual warm nights in Tibet Plateau, southern China, and northwestern China is earlier than northeastern China (Fig. 4–5). All the time of emergence in signals of the other temperature indices is latter than that of warm nights in each region of China (Fig. S7–S8).

Concluding Remarks

Based on six models chosen from CMIP5, we examine bias-corrected multi-model median S/N in temperature extremes over China during 850–2005. Our major conclusions are as follows.

(1) The temporal information of annual temperature extremes in China are consistent with annual mean temperature variations, with larger (smaller) absolute values of regional mean S/N in cold (warm) climatic conditions during 850–1850. The regional mean increasing signals in annual cold nights and cold days in China emerge from natural variability during 1247–1276 and 1810–1828 at the level of S/N > 1.

(2) At local scale, some increasing signals of cold extremes and decreasing signals of warm extremes in most of China especially in southern China and Tibet Plateau exceed natural variability in the second half of the 13th century and in the early 19th century at the level of S/N > 1. Some local increasing signals of cold extremes are also larger than natural variability in the 17th century and in the 18th century. These emerging signals are qualitatively consistent with extremely cold conditions and may be partially due to intensively explosive volcanism during the last millennium.

(3) Over the past 150 years, regional mean decreasing signals of cold extremes and regional mean increasing signals of warm extremes over China emerge from natural variability after 1969 at the level of S/N > 1, and local signals first occur in 1929 in Tibet Plateau. These warming signals may be related to greenhouse gases forcing.

Furthermore, the agreement between the behaviors shown by the reconstructions of LMR and models is the highest during period 1851–2000, and it is higher during 1400–1850 than during 850–1399. First, the minor contribution of volcanic forcing found in LMR is in disagreement with findings for CMIP5 simulations for the period 850–1399. This might partly be due to different responses of volcanic effect in reconstructions and model simulations (Hartl-Meier et al. 2017). Another may be partly due to less proxy records except for the uncertainty of models. Before 1400, the number of global proxy sites is less than 150, and it is between 250 to 450 during the period 1500–1850 (Tardif et al. 2019). Moreover, the proxy records over China are mainly in Tibet Plateau. Second, both reconstructions by LMR and Li et al. (2021) and simulations present that the early 19th century is a cold period, but it is related to the AMO for reconstructions (Ratna et al. 2019, Li et al. 2021) and to volcanic forcing for simulations. This might because that analyzed models lack some critical forcing or have missing or too-weak feedback mechanisms (Ljungqvist et al. 2019). Thus, future work about temperature extremes in China during the last millennium should use more sophistical method to detect internal or external forcing factors (Wang et al. 2018).

Declarations

Acknowledgements This research was supported by National Key Research and Development Program of China (2018YFA0605602 and 2016YFA0602002), and China Postdoctoral Science Foundation (2016M590724).

References

1. Abram NJ, McGregor HV, Tierney JE et al (2016) Early onset of industrial-era warming across the oceans and continents. Nature 536: 411–418
2. Bothe O, Jungclaus JH, Zanchettin D (2013) Consistency of the multi-model CMIP5/PMIP3-past1000 ensemble. Climate of The Past 9: 2471-2487
3. Chen D, Rojas M, Samset BH et al (2021) Framing, context, and methods. In: Climate Change 2021: The Physical Science Basis. Contribution of Working Group I to the Sixth Assessment Report of the Intergovernmental Panel on Climate Change [Masson-Delmotte V, Zhai P, Pirani A et al (eds.)]. In Press
4. Christiansen B, Ljungqvist FC (2017) Challenges and perspectives for large-scale temperature reconstructions of the past two millennia. Rev Geophys 55: 40–96
5. Cook ER, Krusic PJ, Anchukaities KJ et al (2013) Tree-ring reconstructed summer temperature anomalies for temperate East Asia since 800 C.E. Clim Dyn 41: 2957–2972
6. Deser C, Phillips A, Bourdette V, Teng H (2012) Uncertainty in climate change projections: the role of internal variability. Clim Dyn 38: 527–546
7. Eyring V, Bony S, Meehl GA et al (2016) Overview of the Coupled Model Intercomparison Project Phase 6 (CMIP6) experimental design and organization. Geosci Model Dev 9: 1937–1958
8. Frame D, Joshi M, Hawkins E et al (2017) Population-based emergence of unfamiliar climates. Nature Climate Change 7(6): 407–411
9. Ge Q, Hao Z, Zheng J, Shao X (2013) Temperature changes over the past 2000 yr in China and comparison with the Northern Hemisphere. Clim Past 9: 1153–1160
10. Giorgi F, Bi X (2009) Time of emergence (TOE) of GHG-forced precipitation change hot-spots. Geophys Res Lett, 36, L06709, doi:10.1029/2009GL037593
11. Hao Z, Zheng J, Ge Q et al (2011) Historical analogues of the 2008 extreme snow event over Central and Southern China. Clim Res 50: 161–170
12. Hartl-Meier CTM, Büntgen U, Smerdon JE et al (2017) Temperature covariance in tree ring reconstructions and model simulations over the past millennium. Geophys Res Lett 44: 9458–9469
13. Hawkins E, Sutton R (2012) Time of emergence of climate signals. Geophys Res Lett, 39, L01702, doi:10.1029/2011GL050087
14. Li J, Li J, Li T, Au TF (2021) 351-year tree ring reconstruction of the Gongga Mountains winter minimum temperature and its relationship with the Atlantic Multidecadal Oscillation. Climatic Chang 165: 1–19
15. Li D, Yuan J, Kopp RE (2020) Escalating global exposure to compound heat-humidity extremes with warming. Environ. Res. Lett. 15: 064003.
16. Ljungqvist FC, Zhang Q, Brattström G et al (2019) Centennial-Scale Temperature Change in Last Millennium Simulations and Proxy-Based Reconstructions. J Clim 32: 2441–2482

17. Loarie SR, Duffy PB, Hanilton H, et al (2009) The velocity of climate change. Nature 462(7276): 1052–1055
18. Lopez H, West R, Dong S et al (2018) Early emergence of anthropogenically forced heat waves in the western United States and Great Lakes. Nat Clim Change 8: 414–420
19. Lyu S, Li Z, Zhang Y, Wang X (2016) A 414-year tree-ring-based April–July minimum temperature reconstruction and its implications for the extreme climate events, northeast China. Clim Past 12: 1879–1888
20. King AD, Donat MG, Fischer EM et al (2015) The timing of anthropogenic emergence in simulated climate extremes. Environ Res Lett 10:094015
21. Mahlstein I, Knutti R, Solomon S, Portmann RW (2011) Early onset of significant local warming in low latitude countries. Environ Res Lett doi:10.1088/1748-9326/6/3/034009
22. Masson-Delmotte V, Schulz M, Abe-Ouchi A et al (2013) Information from Paleoclimate Archives. In: Stocker TF, Qin D, Plattner G-K et al (eds) Climate change 2013: The physical science basis contribution of working group I to the fifth assessment report of the intergovernmental panel on climate change. Cambridge University Press, Cambridge, United Kingdom and New York, NY, USA, pp 383–464
23. Mora C, Frazier AG, Longman RJ et al (2013) The projected timing of climate departure from recent variability. Nature 502: 183–187
24. Nguyen T-H, Min S-K, Paik S, Lee D (2018) Time of emergence in regional precipitation changes: an updated assessment using the CMIP5 multi-model ensemble. Clim Dyn 51: 3179–3193
25. Ratna SB, Osborn TJ, Joshi M, Yang B, Wang J (2019) Identifying teleconnections and multidecadal variability of East Asian surface temperature during the last millennium in CMIP5 simulations. Clim Past 15: 1825–1844
26. Schmidt GA, Jungclaus JH, Ammann CM et al (2011) Climate forcing reconstructions for use in PMIP simulations of the last millennium (v1.0). Geosci Model Dev 4: 33–45
27. Shi F, Ge Q, Yang B et al (2015) A multi-proxy reconstruction of spatial and temporal variations in Asian summer temperatures over the last millennium. Climatic Change 131: 663–676
28. Sillmann J, Kharin VV, Zwiers FW, Zhang X, Bronaugh D (2013) Climate extremes indices in the CMIP5 multimodel ensemble: Part 1. Model evaluation in the present climate. J Geophys Res Atmos 118: 1–18. doi:10.1002/jgrd.50203.
29. Sueyoshi T, Ohgaito R, Yamamoto A, et al (2012) Set-up of the PMIP3 paleoclimate experiments conducted using an Earth system model, MIROC-ESM. Geosci Model Dev 6: 819–836
30. Sui Y, Lang X, Jiang D (2014) Time of emergence of climate signals over China under the RCP4.5 scenario. Climatic Change 125: 265–276
31. Sui Y, Lang X, Jiang D (2018) Projected signals in climate extremes over China associated with a 2 ∘C global warming under two RCP scenarios. Int J Climatol 38: e678–e697

32. Tardif R, Hakim GJ, Perkins WA et al (2019) Last Millennium Reanalysis with an expanded proxy database and seasonal proxy modeling. Clim Past 15: 1251–1273
33. Taylor KE, Stouffer RJ, Meehl GA (2012) An overview of CMIP5 and the experiment design. Bull Amer Meteorol Soc 93: 485–498
34. Wang J, Yang B, Osborn TJ, et al (2018) Causes of East Asian temperature multidecadal variability since 850 CE. Geophys Res Lett 45: 13485–13494
35. Wang S, Wen X, Luo Y et al (2007) Reconstruction of temperature series of China for the last 1000 years. Chinese Sci Bull 52(23): 3272–3280
36. Wu J, Gao X (2013) A gridded daily observation dataset over China region and comparison with the other datasets. Chin J Geophys 56: 1102–1111 (in Chinese)
37. Yang B, Braeuning A, Johnson KR, Shi YF (2002) General characteristics of temperature variation in China during the last two millennia. Geophys Res Lett 29: 1324, doi:10.1029/2001GL014485
38. Zhang D (2004) A Compendium of Chinese Meteorological Records of the Last 3,000 Years. Nanjing: Jiangsu Education Press, 1–3666
39. Zhang D, Gaston D (2004) Northern China maximum temperature in the summer of 1743: A historical event of burning summer in a relatively warm climate background. Chinese Sci Bull 49: 2508–2514
40. Zhang H, Werner JP, García-Bustamante E, et al (2018) East Asian warm season temperature variations over the past two millennia. Scientific Reports 8: 7702. doi:10.1038/s41598-018-26038-8
41. Zhang X, Hegerl G, Zwiers FW, Kenyon J (2005) Avoiding inhomogeneity in percentile-based indices of temperature extremes. J Clim 18: 1641–1651
42. Zheng J, Ding L, Hao Z, Ge Q (2012) Extreme cold winter events in southern China during AD 1650–2000. Boreas 41: 1–12

Tables

Table 1 Basic information on seven CMIP5 models and two CMIP6 models and their experiments

Model name	Country or Institution	CMIPs	Atmospheric Resolution	Length of run analyzed (period in model year)		
				Pre-industrial control	Historical	Past1000
BCC-CSM1.1	China	CMIP5	128 × 64, L26	301–500, 200	1850–2005	850–1850
CCSM4	USA	CMIP5	288 × 192, L26	953–1108, 156	1850–2005	850–1850
CSIRO-Mk3L-1-2	Australia	CMIP5	64 × 56, L18	951–1000, 50	1851–2005	851–1850
IPSL-CM5A-LR	France	CMIP5	96 × 95, L39	2600–2799, 200	1850–2005	1050–1850
MPI-ESM-P	Germany	CMIP5	196 × 98, L47	2806–3005, 200	1850–2005	850–1849
MRI-CGCM3	Japan	CMIP5	320 × 160, L48	2151–2350, 200	1850–2005	850–1850
MIROC-ESM	Japan	CMIP5	128 × 64, L80	2230–2429, 200	1850–2005	850–1849
MRI-ESM2.0	Japan	CMIP6	320 × 160, L80	1850–2049, 200	1850–2014	850–1849
EC-Earth3-Veg-LR	EC-Earth-Consortium	CMIP6	320 × 160, L62	2151–2350, 200	1850–2014	850–1849

Table 2 Information on the 12 temperature indices analyzed in this work. Here, TN_{ij}, and TX_{ij} denote daily minimum and maximum temperatures on day *i* in period *j*, respectively. The base period refers to 1961–1990.

Index name (label)	Units	Index definition
Coldest night (TNn)	°C	The minimum daily minimum temperature
Warmest night (TNx)	°C	The maximum daily minimum temperature
Coldest day (TXn)	°C	The minimum daily maximum temperature
Hottest day (TXx)	°C	The maximum daily maximum temperature
Tropical nights (TR)	Days	The number of days when $TN_{ij} > 20°C$
Frost days (FD)	Days	The number of days when $TN_{ij} < 0°C$
Summer days (SU)	Days	The number of days when $TX_{ij} > 25°C$
Icing days (ID)	Days	The number of days when $TX_{ij} < 0°C$
Warm nights (TN90p)	Days	The number of days when $TN_{ij} > TN_{in}90$; here, $TN_{in}90$ is the calendar day 90th percentile centered on a 5-day window for the base period
Cold nights (TN10p)	Days	The number of days when $TN_{ij} < TN_{in}10$; here, $TN_{in}10$ is the calendar day 10th percentile centered on a 5-day window for the base period
Warm days (TX90p)	Days	The number of days when $TX_{ij} > TX_{in}90$; here, $TX_{in}90$ is the calendar day 90th percentile centered on a 5-day window for the base period
Cold days (TX10p)	Days	The number of days when $TX_{ij} < TX_{in}10$; here, $TX_{in}10$ is the calendar day 10th percentile centered on a 5-day window for the base period

Table 3 The correlation coefficients between bias-correctted multi-model median S/N of cold nights and the radiative forcings from individual components: well-mixed greenhouse gases (CO_2, CH_4 and N_2O combined), volcanic aerosols (two reconstructions), and solar TSI (six reconstructions) for periods 900–1200, 1201–1449, 1450–1850, and 1851–2000.

	greenhouse gases	volcanic aerosols	solar TSI
900–1200	0.21	−0.50	−0.07
1201–1449	0.17	−0.95	−0.07
1450–1850	−0.16	−0.54	0.27
1851–2000	−0.96	0.07	−0.59

Figures

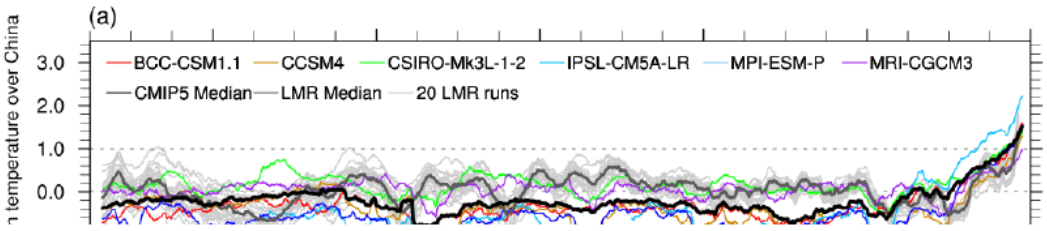

Figure 1

Relative to the pre-industrial control run, 31-year periods of bias-corrected S/N for six models and their multi-model median in annual (a) daily mean temperature, (b) cold nights (TN10p), and (c) warm nights (TN90p) during 850–2005 in China, and (d) estimated radiative forcings from individ-ual components:

well-mixed greenhouse gases (CO2, CH4 and N2O combined), volcanic aerosols (two reconstructions), and solar TSI (six reconstructions) for the PMIP period 850–2000. Relative to the period 1651–1850, 31-year periods of S/N in annual mean temperature for 20 ensemble-mean values for each Monte-Carlo reconstruction from Last Millennium Reanalysis reconstruction (LMR) and their multi-model median during 850–2000 in China are also presented in panel (a).

Figure 2

Relative to the pre-industrial control run, ratios of areas where the absolute values of bias-corrected S/N are larger than 1 to the whole country for six models and their multi-model median in annual (a) daily mean temperatures, (b) cold nights (TN10p), and (c) warm nights (TN90p) during 850–2005 in China. The positive ratios indicate S/N are larger than 1, and the negative ratios indicate S/N are smaller than –1. “M1”, “M2”, “M3”, “M4”, “M5”, “M6”, and “Med” indicate BCC-CSM1.1, CCSM4, CSIRO-Mk3L-1-2, IPSL-CM5A-LR, MPI-ESM-P, MRI-CGCM3, and multi-model me-dian, respectively.

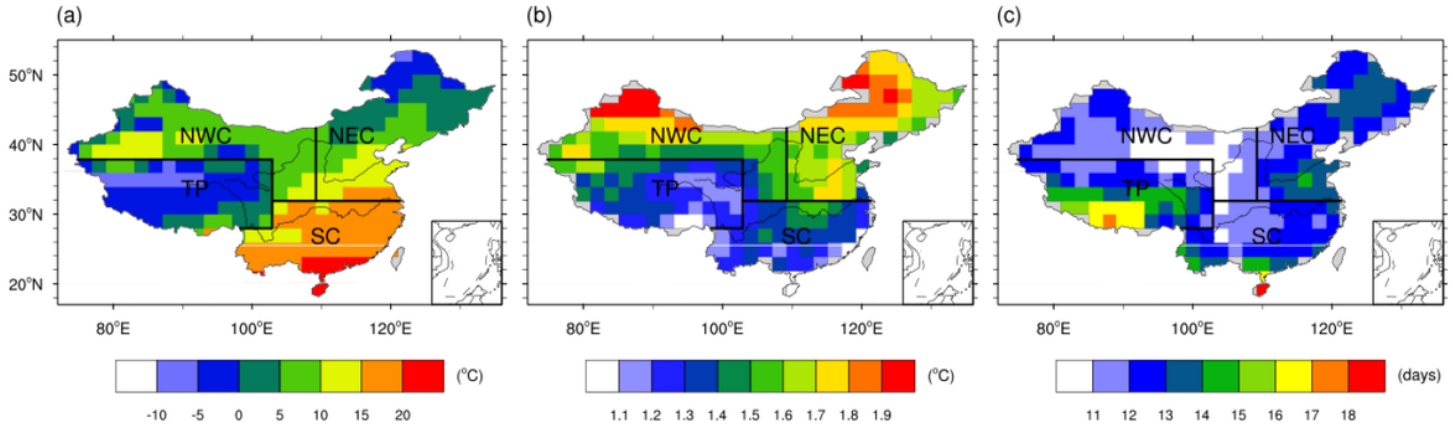

Figure 3

The spatial pattern of (a) bias-corrected median in annual mean temperature over China during peri-od 1975-2005 based on six CMIP5 models, (b) average of bias-corrected median noises in annual mean minimum and maximum temperatures, coldest night (TNn), warmest night (TNx), coldest day (TXn) and hottest day (TXx), and (c) average of bias-corrected median noises in annual cold nights (TN10p), warm nights (TN90p), cold days (TX10p) and warm days (TX90p) over China derived from pre-industrial control run of six CMIP5 models. Domains of four roughly equal area subregions in China are presented in each panel. NWC: northwestern China; NEC: northeastern China; TP: Ti-bet Plateau; and SC: southern China.

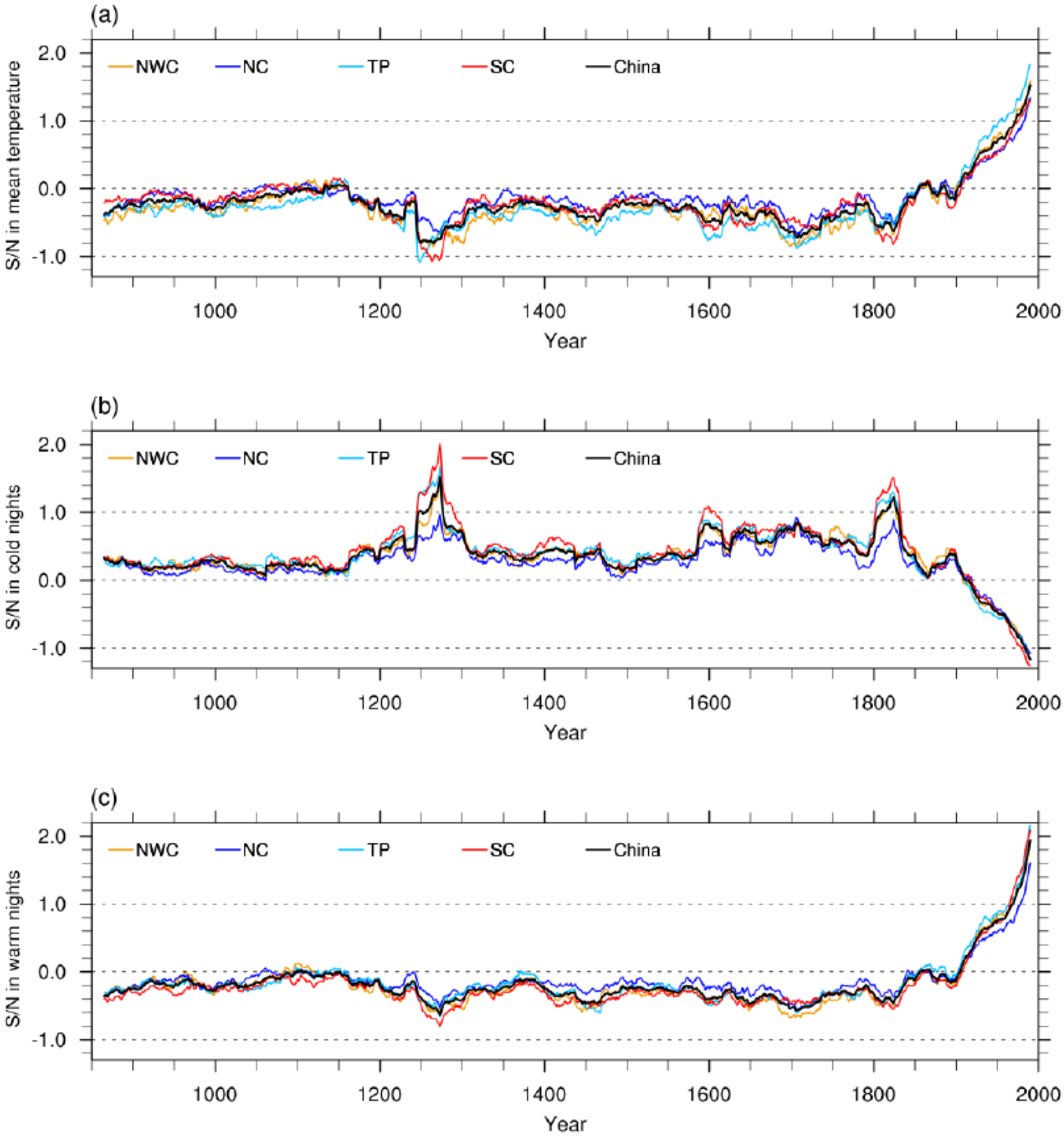

Figure 4

Relative to the pre-industrial control run, 31-year periods of bias-corrected multi-model median S/N in annual (a) daily mean temperature, (b) cold nights (TN10p), and (c) warm nights (TN90p) during 850–2005 for four regions (shown in Fig. 3) in China.

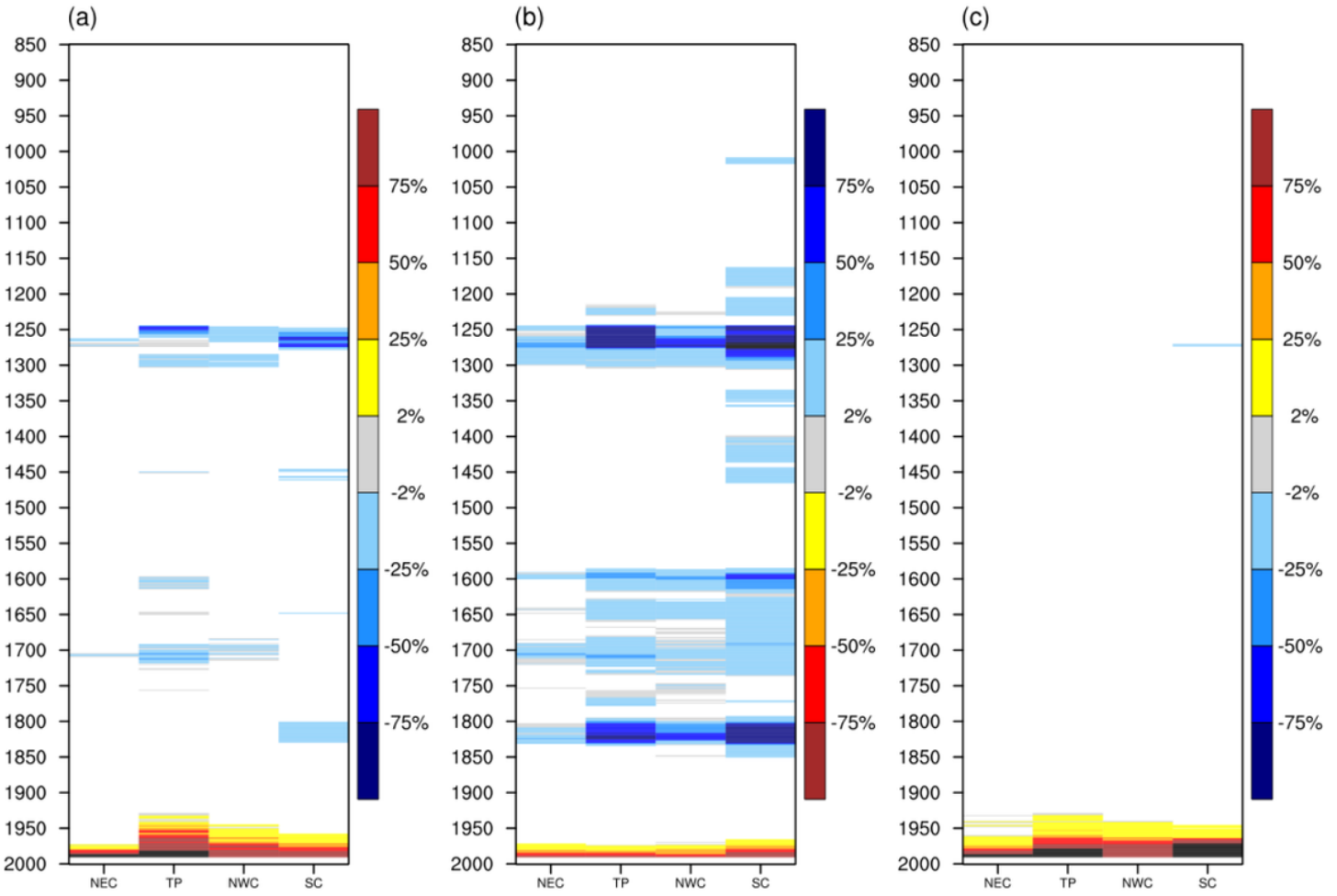

Figure 5

Relative to the pre-industrial control run, ratios of areas where the absolute values of bias-corrected S/N are larger than 1 to each whole region for multi-model median in annual (a) daily mean temper-atures, (b) cold nights (TN10p), and (c) warm nights (TN90p) during 850–2005 in four regions (shown in Fig. 3) of China. The positive ratios indicate S/N are larger than 1, and the negative ratios indicate S/N are smaller than −1.

Supplementary Files

This is a list of supplementary files associated with this preprint. Click to download.

- 20211116supplymentarymaterialrevised.doc